Rheological Dynamics of Active Myxococcus xanthus Populations during Development

Matthew E. Black and Joshua W. Shaevitz*

Joseph Henry Laboratories of Physics and the Lewis-Sigler Institute for Integrative Genomics, Princeton University, Princeton, New Jersey 08544, USA

(Received 24 November 2021; accepted 21 March 2023; published 24 May 2023)

The bacterium Myxococcus xanthus produces multicellular droplets called fruiting bodies when starved. These structures form initially through the active dewetting of a vegetative biofilm into surface-associated droplets. This motility-driven aggregation is succeeded by a primitive developmental process in which cells in the droplets mature into nonmotile spores. Here, we use atomic force microscopy to probe the mechanics of these droplets throughout their formation. Using a combination of time- and frequency-domain rheological experiments, we characterize and develop a simple model of the linear viscoelasticity of these aggregates. We then use this model to quantify how cellular behaviors predominant at different developmental times-motility during the dewetting phase and cellular sporulation during later development—manifest as decreased droplet viscosity and increased elasticity, respectively.

DOI: 10.1103/PhysRevLett.130.218402

Populations of the bacterium Myxococcus xanthus form an active fluid that wets solid surfaces and allows cells to spread and predate on other species. When food is scarce, cell division ceases and this fluid dewets from the substrate to form droplet-shaped mounds inside of which a fraction of the population differentiates into chemically and mechanically resilient spores [1]. The resultant macroscopic structure, a fruiting body, acts as a linchpin in the social lifestyle of M. xanthus by maintaining the spore population as a coherent whole against physical and chemical stresses from the environment [2,3]. While considerable work has investigated the genetic underpinnings of fruiting body morphogenesis, a physical basis for how these structures form during the dewetting of the cell population, and the mechanical properties that allow them to fulfill their ultimate ecological function, remain unknown. To address this deficit, we used atomic force microscopy (AFM) to probe the rheology of M. xanthus aggregates throughout their development from a dewetted droplet to a mature, spore-filled fruiting body [Figs. 1(a) and 1(b)].

Fruiting bodies were grown on glass coverslips following Ref. [4] (see Supplemental Material [5], section S2A). Nascent droplets were first identifiable from the wetted cell population 12 h after the onset of starvation in a nutrientless buffer solution. Fruiting-body formation takes place in two phases (Fig. S1). Growth of the aggregate occurs first and is

Published by the American Physical Society under the terms of the Creative Commons Attribution 4.0 International license. Further distribution of this work must maintain attribution to the author(s) and the published article's title, journal citation, and DOI.

then followed by sporulation of the cells. Cells transition from their vegetative lifestyle to the fruiting body growth phase by both (i) ceasing cell growth and division and

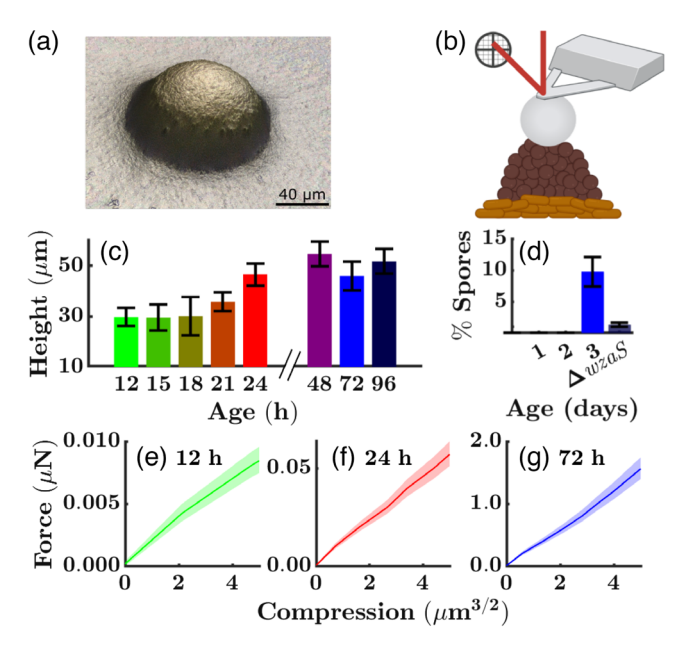


FIG. 1. (a) Three-dimensional image of a typical fruiting body after 48 h of starvation. (b) Experimental schematic. A bead approximately the same size as the droplet is attached to the end of an AFM cantilever to distribute the compressive forces. (c) Fruiting body height plateaus 24 h poststarvation. (d) Sporulation occurs three days after starvation and is greatly reduced in the Δ wzaS mutant. Sporulation measured after 72 h for the Δ wzaS mutant. Full data is shown in Table S4. (e)–(g) Force as a function of compression at difference times poststarvation (12 h, green, N = 3; 24 h, red, N = 3; 72 h, blue, N = 4). Shaded regions are 90% confidence intervals.

We attached $80 \mu m$ -diameter borosilicate glass beads to tipless AFM cantilevers and applied compressive forces from above [Fig. 1(b)]. This ensures that the force imposed by the AFM is distributed across the entire droplet. To minimize adhesion and other surface effects, beads were treated with a siliconizing reagent prior to their attachment to the AFM cantilevers (section S2C1, Fig. S5).

We first determined the appropriate contact model for this geometry by measuring the force-compression relationship for aggregates 12, 24, and 72 h poststarvation in the linear contact regime [16]. Contact was well-approximated as Hertzian, where the imposed force, F, scales linearly with sample compression, δ , to the three-halves power [Figs. 1(e)–1(g)]. To account for the hemielliptical shape of each droplet, a small correction factor ($\beta \approx 0.97$ –0.99) is introduced into the contact model [17] (section S2D1). We assume that the droplets remain incompressible throughout development. Force and compression are thus related by

$$F = \frac{16\sqrt{R_c}}{9\beta}E\delta^{3/2},\tag{1}$$

where E is the droplet's Young's modulus and R_c is the radius of the (uncorrected) spherical contact area between the cantilever-attached glass bead and the droplet surface.

We observe a dramatic increase in aggregate stiffness over the developmental process. While 12-h aggregates have apparent Young's moduli of 0.24 ± 0.06 kPa [Fig. 1(e)], mature fruiting bodies are over 2 orders of magnitude stiffer, $E=36.6\pm15$ kPa [Fig. 1(g)]. Fully dewetted, but not-yet-sporulated, aggregates at 24 h displayed an intermediate stiffness [$E=3.7\pm1.5$ kPa, Fig. 1(f)], suggesting that the growth process occurs alongside other processes that cause stiffening.

Because droplet growth is driven by cell motility, we hypothesized that aggregates would exhibit liquidlike flow at timescales characteristic of cellular motion. *M. xanthus* cells move at a speed of about one body length per minute and reverse their direction with a characteristic timescale of tens to hundreds of seconds [13]. To probe these timescales, we adapted previously developed methods [18,19] to measure complex moduli over a frequency range spanning

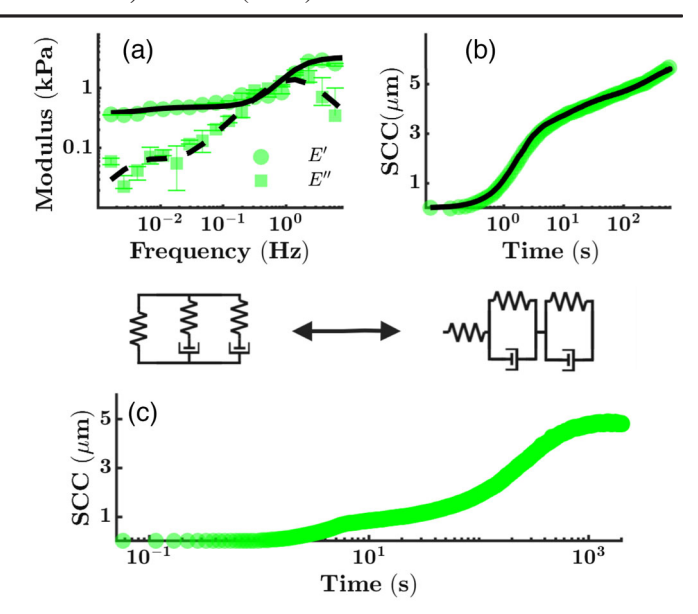


FIG. 2. (a) Dynamic modulus as a function of frequency for a single 12-h aggregate (green), and resultant least-squares fit (black) to a two-element Wiechert model, shown below the graph. Error bars represent the smallest and largest moduli calculated from the fit coefficient confidence intervals. (b) Compression (creep) time series for the same aggregate as in (a) under a constant compressive force of 60 nN (green), and the resulting fit to the spring-dashpot model shown below (black). Compression is plotted as $SCC = \delta^{3/2}/\sqrt{R_c}$ (see text). (c) Creep experiment demonstrating an equilibrium plateau in compression at very long times, $\sim 10^3$ s.

1 mHz to 10 Hz (sections S2C, S2D2). Over this frequency range, droplets are viscoelastic [Figs. 2(a) and 3] and exhibit two relaxation timescales at \sim 1 s and \sim 100 s. This linear viscoelastic behavior can be described using a two-element Wiechert model with complex modulus [20],

$$E^*(\omega) = E_{\infty} + \frac{E_1 \tau_1 i \omega}{1 + \tau_1 i \omega} + \frac{E_2 \tau_2 i \omega}{1 + \tau_2 i \omega}, \tag{2}$$

where E_{∞} is the equilibrium modulus and the pairs (E_1, τ_1) and (E_2, τ_2) are the moduli and relaxation times of the short- and long-time relaxation modes.

We confirmed the relevance of this model by performing time-domain creep experiments, where the AFM is used to apply a fixed load and the resulting compression over time is recorded (section S2E). Guided by Eq. (1), we define a size-corrected compression, $SCC \equiv \delta^{3/2}/\sqrt{R_c}$, and monitor its evolution over time [Figs. 2(b) and 2(c)]. In creep, nascent droplets show flow over timescales characteristic of cell motility [Fig. 2(b)] and an equilibrium plateau at long times as predicted by the Kelvin-Voigt model [Fig. 2(c)]. This model is the exactly equivalent conjugate model to the Wiechert model used to fit the frequency-domain data (S3).

To extract model parameters from these experiments, the times series SCC(t) for each experiment was fit to the

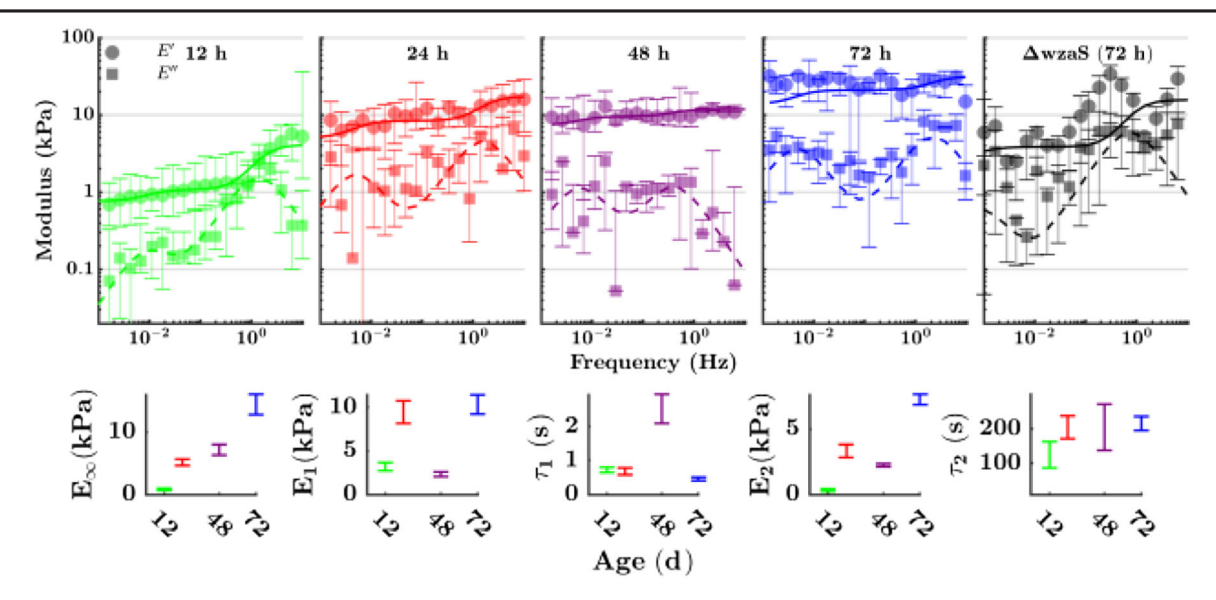


FIG. 3. (Top) Dynamic modulus of fruiting bodies over the course of development. Points shown are median values for storage (E') and loss (E'') moduli at each frequency, taken across all experiments. N=4, 20, 6, 19 for ages 12, 24, 48, and 72 h poststarvation, respectively. N=7 for the Δ wzaS mutant at 72 h poststarvation. Lines are least-squares fits to Eq. (2) of the complex modulus over all frequencies (solid and dashed lines correspond with the storage and loss moduli, respectively). (Bottom) The change in each fit parameter is shown over the course of development. Error bars are bootstrapped 95% confidence intervals.

Lee-Radok solution for viscoelastic contact with timeincreasing contact area [21],

$$\frac{\delta^{3/2}(t)}{\sqrt{R_c}} = \frac{9\beta}{16} \int_0^t J(t-\tau) \frac{dF}{d\tau} d\tau. \tag{3}$$

J(t) is the creep compliance function,

$$J(t) = J_0[1 + q_1(1 - e^{-t/\lambda_1}) + q_2(1 - e^{-t/\lambda_2})], \quad (4)$$

where λ_1 , λ_2 are the two retardation times with corresponding compliances J_0q_1 and J_0q_2 [20].

We next measured the complex modulus of fruiting bodies over the course of development to ask how the apparent modulus changes described earlier manifest themselves rheologically. Similar to our earlier findings [Figs. 1(e)-1(g)], the low frequency storage moduli of developing aggregates increases by more than an order of magnitude over the course of development. This absolute change in modulus takes place without significant changes to the relative viscoelastic response, as evidenced by an apparent equilibrium modulus at the lowest measured frequencies and two, well-separated relaxation timescales at ~1 s and ~100 s that remain separated and of similar magnitude for all ages (Fig. 3). Analysis of the change in each parameter between age groups by one-way analysis of variance reveals statistically significant trends (p < 0.05) for both E_2 and the equilibrium modulus, E_{∞} .

To test whether these changes were driven by the biological developmental process, we imposed oscillatory measurements on the nonsporulating mutant Δ wzaS at the

72-h time point. This mutant strain lacks the protein responsible for exporting the major spore coat polymer across the outer membrane, and ultimately causes cells to abort their differentiation into spores [22,23]. Three days poststarvation, aggregates from this strain only contain $1.3 \pm 0.3\%$ spores, compared to $9.8 \pm 2.3\%$ for wild-type *M. xanthus* [Fig. 1(d), Table S4).

This strain has a nearly fivefold reduction in the elastic modulus at low frequencies relative to the wild type (Fig. 3). We find a statistically significant difference between the equilibrium moduli of Δ *wzaS* and wild type $(E_{\infty}^{\Delta wzaS} < E_{\infty}^{\text{wild-type}})$, p < 0.05 by Wilcoxon signed-rank test). Relative to wild type, this strain also shows a fourfold increase in relaxation time, τ_2 (Table S1), suggesting that aggregate viscosity is not affected by sporulation in the same manner as elasticity.

While droplet viscoelasticity evolves throughout the developmental process, changes are especially rapid during the initial dewetting phase between 12 and 24 h post-starvation. The speed at which these changes take place, combined with the low frequencies where they occur, preclude us from making frequency-sweep measurements at intermediate ages that avoid effects from sample evolution [24]. For example, a single frequency-sweep experiment, covering frequencies from 1 mHz to 10 Hz takes approximately 1.5 h. To probe aggregate viscoelasticity during these early stages, we performed 10 m long creep experiments, allowing us to measure changes in aggregate flow and compliance on shorter times. Measurements done at 3 h intervals during the initial dewetting period show that changes in both the instantaneous stiffness, J_0^{-1} , and low

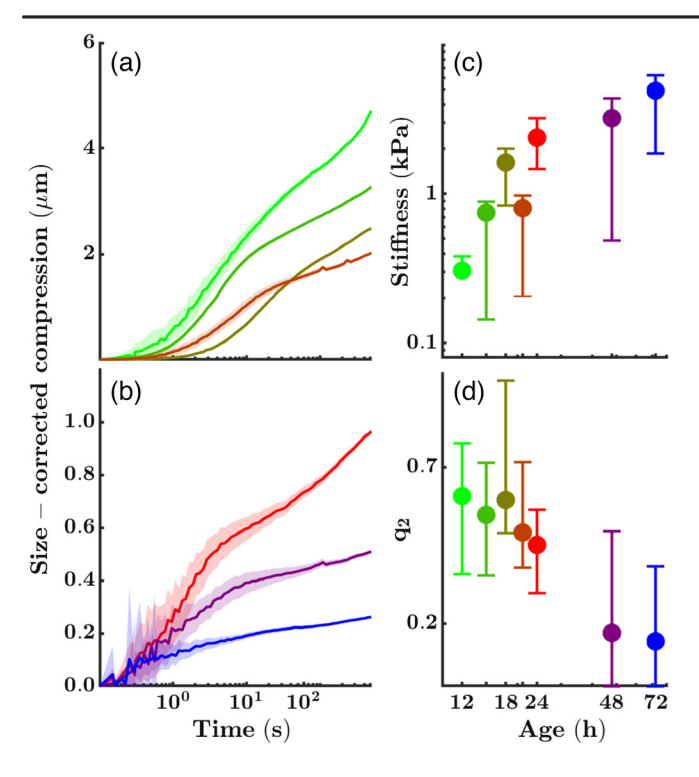


FIG. 4. (a),(b) Mean creep curves for early [(a) 12, 15, 18, and 21 h poststarvation, N=13,4,7,7, respectively) and late [(b) 24, 48, 72 h poststarvation, N=12,10,13, respectively) development. Colors are defined in panels (c),(d). Shaded regions are ± 1 standard deviation. (c),(d) The stiffness, J_0^{-1} , and long-timescale relative stiffness, q_2 , as a function of age. Error bars are 95% confidence intervals.

frequency compliance, q_2 , occur at an approximately constant rate over this period [Figs. 4(c) and 4(d)]. Tables S2 and S3 show the best-fit model parameter values for droplets between 12 and 72 h poststarvation.

The creep curves for nascent droplets all share a similarly shaped response with an initial deformation followed by an approximate doubling of the deformation due to subsequent creeping flow [Fig. 4(a)]. At later times [Fig. 4(b), 48 and 72 h) the same degree of creeping flow is not present. Given the correspondence between this arrest in creeping flow and droplet growth after 24 h of starvation, and the fact that droplet growth is driven by cell motility, we hypothesized that cell motion generates viscous flows and fluidizes nascent droplets.

To test this hypothesis, we performed consecutive creep experiments on developing fruiting bodies before and after exposure to 20 µm of the motility-halting drug carbonyl cyanide-m-chlorophenylhydrazone (CCCP, S2B). CCCP is a proton ionophore that rapidly destroys the cellular proton motive force, causing motility to cease within minutes [25,26]. While CCCP can affect other aspects of cellular physiology such as an inhibition of cell growth and division, the starving *M. xanthus* cells in our experiments are not growing so that the dominant effect of this drug is a change in motility.

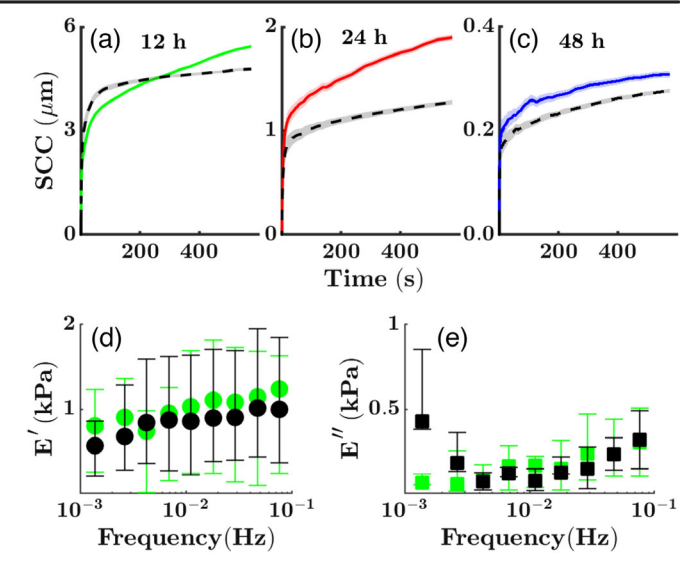


FIG. 5. (a)–(c) Mean creep curves pretreatment (colored solid lines) and post-treatment (black dashed) with the motility-halting drug CCCP. Shaded regions are ± 1 standard deviation. N=4,7,5 for (a), (b), and (c), respectively. Storage (d) and loss (e) moduli for 12 h poststarvation droplets before (green) and after (black) CCCP exposure (N=4).

Treatment with CCCP suppressed much of the late-time creeping flow in 12- and 24-h droplets, yielding a response similar to 48-h fruiting bodies in which the sporulation transition is underway and cell motility is naturally reduced [Figs. 5(a) and 5(b), S4]. Treatment with CCCP did not similarly affect the creep response of 48-h poststarvation droplets [Fig. 5(c)], with only a minor change in absolute flow and the general shape of the response being preserved pre- and post-treatment. We attribute the suppression of long-time flow to a viscosity reduction brought on by cell motility. This is consistent with an approximately fivefold increase in E'' for 12-h droplets at low frequencies that we observe after exposure to CCCP [Fig. 5(e)], whereas E' remains unaffected by the drug across all frequencies [Fig. 5(d)].

A reduction in the loss modulus of nascent droplets due to cell motility suggests that activity fluidizes the system, similar to phenomena in dilute suspensions of active extensile particles [27,28]. We have previously observed that wetted layers of *M. xanthus* are nematically ordered [29]. Activity-driven fluidization may thus indicate that droplets also retain nematic order, so that activity acts to reinforce material flow [30]. This is supported by a recent imaging study that reported high degrees of nematic orientational order in droplets up to 1 d poststarvation [31].

We also observe a dramatic stiffening of the aggregate during the first day poststarvation along with the substantial flows. While we were not able to tease apart a biological mechanism for this observed early stiffening, that it cooccurs with material flow suggests that its source is likely not due to changes in the nematic structure of the material or motility, but instead may be due to cellular anabolism.

The excretion of an extracellular matrix (ECM), a complex mix of polysaccharides, proteins, and extracellular DNA, is known to be essential for fruiting body formation [32,33] and has been suggested to form a structural scaffold within the fruiting body [34–36]. The formation of the ECM over time may explain part of the stiffening we observe during early fruiting body maturation. It is possible that, similar to in biofilms of other gram-negative bacteria, the short timescale we observe, $\tau_1 \sim 1$ s, corresponds to the viscoelastic relaxation time of the polymeric ECM [37].

The measured stiffness difference between the wild-type and nonsporulating Δ wzaS mutant after 72 h of starvation suggests that the elasticity of the cells themselves may also contribute to droplet rheology. Early-stage droplets contain mostly vegetative cells whereas after maturation, fruiting bodies are composed of less-compliant spores. Vegetative M. xanthus cells have been measured to have a Young's modulus of 0.25 ± 0.18 Mpa [38]. While the stiffness of individual M. xanthus spores has not been measured, spores from other bacterial species have been found to have Young's moduli in the range of 0.1-20 GPa, orders of magnitude higher than vegetative cells from those species or M. xanthus [39,40]. The net rheological behavior of mature M. xanthus fruiting bodies is thus likely a product of both the elasticity of single cells and spores, and the polymer matrix formed by extracellular products that those cells excrete, similar to other bacterial aggregates and biofilms [41].

Altogether, our work presents a picture of fruiting body development in which starvation-induced changes in cellular physiology drive changes in droplet rheology. Cell flows are integral to the dewetting process seen in early fruiting body formation and we have shown that cell motility enables this by fluidizing the material. At later stages of development, the fruiting body becomes much stiffer. We attribute this change, in part, to the formation of mechanically stiff spores. We hypothesize that these rheological changes allow *M. xanthus* fruiting bodies to fulfill their proposed biological function in maintaining the spore population, suggesting an intimate link between the mechanics and social lifestyle of the myxobacteria.

The authors thank Katherine Copenhagen, Endao Han, and Cassidy Yang for helpful discussions. This work was supported by the National Science Foundation through the Center for the Physics of Biological Function (PHY-1734030) and Grant PHY-1806501.

- *Corresponding author. shaevitz@princeton.edu
- K. A. O'Connor and D. R. Zusman, Development in Myxococcus xanthus involves differentiation into two cell types, peripheral rods and spores, J. Bacteriol. 173, 3318 (1991).
- [2] J. MUÑOZ-Dorado, F. J. Marcos-Torres, E. García-Bravo, A. Moraleda-Muñoz, and J. Pérez, Myxobacteria: Moving,

- killing, feeding, and surviving together, Front. Microbiol. **7**, 781 (2016).
- [3] K. Lee and L. J. Shimkets, Cloning and characterization of the socA locus which restores development to Myxococcus xanthus C-signaling mutants, J. Bacteriol. **176**, 2200 (1994).
- [4] J. Kuner and D. Kaiser, Fruiting body morphogenesis in submerged cultures of Myxococcus xanthus., J. Bacteriol. 151, 458 (1982).
- [5] See Supplemental Material at http://link.aps.org/ supplemental/10.1103/PhysRevLett.130.218402, which includes Refs. [6–11], for additional information on experimental methods, tabulated results, and our contact and viscoelastic models.
- [6] D. E. Whitworth *et al.*, *Myxobacteria*. *Multicellularity and Differentiation*. (ASM press, Washington, DC, 2008).
- [7] Y.-R. Chang, V. K. Raghunathan, S. P. Garland, J. T. Morgan, P. Russell, and C. J. Murphy, Automated AFM force curve analysis for determining elastic modulus of biomaterials and biological samples, J. Mech. Behav. Biomed. Mater. 37, 209 (2014).
- [8] J. Schindelin, I. Arganda-Carreras, E. Frise, V. Kaynig, M. Longair, T. Pietzsch, S. Preibisch, C. Rueden, S. Saalfeld, B. Schmid *et al.*, Fiji: An open-source platform for biological-image analysis, Nat. Methods 9, 676 (2012).
- [9] J. F. Brenner, B. S. Dew, J. B. Horton, T. King, P. W. Neurath, and W. D. Selles, An automated microscope for cytologic research a preliminary evaluation., J. Histochem. Cytochem. 24, 100 (1976).
- [10] Y. M. Efremov, W.-H. Wang, S. D. Hardy, R. L. Geahlen, and A. Raman, Measuring nanoscale viscoelastic parameters of cells directly from AFM force-displacement curves, Sci. Rep. 7, 1 (2017).
- [11] S. Park and R. Schapery, Methods of interconversion between linear viscoelastic material functions. I part a numerical method based on prony series, Int. J. Solids Struct. **36**, 1653 (1999).
- [12] R. Mercier and T. Mignot, Regulations governing the multicellular lifestyle of Myxococcus xanthus, Curr. Opin. Microbiol. 34, 104 (2016).
- [13] G. Liu, A. Patch, F. Bahar, D. Yllanes, R. D. Welch, M. C. Marchetti, S. Thutupalli, and J. W. Shaevitz, Self-Driven Phase Transitions Drive Myxococcus xanthus Fruiting Body Formation, Phys. Rev. Lett. 122, 248102 (2019).
- [14] L. Kroos and D. Kaiser, Expression of many developmentally regulated genes in Myxococcus depends on a sequence of cell interactions, Genes Dev. 1, 840 (1987).
- [15] D. R. Zusman, A. E. Scott, Z. Yang, and J. R. Kirby, Chemosensory pathways, motility and development in Myxococcus xanthus, Nat. Rev. Microbiol. 5, 862 (2007).
- [16] M. Radmacher, Studying the mechanics of cellular processes by atomic force microscopy, Methods Cell Biol. 83, 347 (2007).
- [17] K. L. Johnson, Contact Mechanics (Cambridge University Press, Cambridge, England, 1987).
- [18] G. Huang, B. Wang, and H. Lu, Measurements of viscoelastic functions of polymers in the frequency-domain using nanoindentation, Mech. Time-Depend. Mater. **8**, 345 (2004).
- [19] R. Mahaffy, S. Park, E. Gerde, J. Käs, and C.-K. Shih, Quantitative analysis of the viscoelastic properties of thin

- regions of fibroblasts using atomic force microscopy, Biophys. J. **86**, 1777 (2004).
- [20] N. W. Tschoegl, *The Phenomenological Theory of Linear Viscoelastic Behavior: An Introduction* (Springer Science & Business Media, New York, 2012).
- [21] E. Lee and J. R. M. Radok, The contact problem for viscoelastic bodies, J. Appl. Mech. 27, 438 (1960).
- [22] C. Holkenbrink, E. Hoiczyk, J. Kahnt, and P. I. Higgs, Synthesis and assembly of a novel glycan layer in Myxococcus xanthus spores, J. Biol. Chem. 289, 32364 (2014).
- [23] F.-D. Müller, A. Treuner-Lange, J. Heider, S. M. Huntley, and P. I. Higgs, Global transcriptome analysis of spore formation in Myxococcus xanthus reveals a locus necessary for cell differentiation, BMC Genomics 11, 1 (2010).
- [24] M. Mours and H. Winter, Time-resolved rheometry, Rheol. Acta 33, 385 (1994).
- [25] M. Wartel, A. Ducret, S. Thutupalli, F. Czerwinski, A.-V. Le Gall, E. M. Mauriello, P. Bergam, Y. V. Brun, J. Shaevitz, and T. Mignot, A versatile class of cell surface directional motors gives rise to gliding motility and sporulation in Myxococcus xanthus, PLoS Biol. 11, e1001728 (2013).
- [26] B. Nan, J. Chen, J. C. Neu, R. M. Berry, G. Oster, and D. R. Zusman, Myxobacteria gliding motility requires cytoskeleton rotation powered by proton motive force, Proc. Natl. Acad. Sci. U.S.A. 108, 2498 (2011).
- [27] V. A. Martinez, E. Clément, J. Arlt, C. Douarche, A. Dawson, J. Schwarz-Linek, A. K. Creppy, V. Škultéty, A. N. Morozov, H. Auradou *et al.*, A combined rheometry and imaging study of viscosity reduction in bacterial suspensions, Proc. Natl. Acad. Sci. U.S.A. 117, 2326 (2020).
- [28] D. Saintillan, Rheology of active fluids, Annu. Rev. Fluid Mech. 50, 563 (2018).
- [29] K. Copenhagen, R. Alert, N.S. Wingreen, and J.W. Shaevitz, Topological defects promote layer formation in Myxococcus xanthus colonies, Nat. Phys. 17, 211 (2021).
- [30] Y. Hatwalne, S. Ramaswamy, M. Rao, and R. A. Simha, Rheology of Active-Particle Suspensions, Phys. Rev. Lett. 92, 118101 (2004).

- [31] Y. Hoang, J. L. Franklin, Y. S. Dufour, and L. Kroos, Cell density, alignment, and orientation correlate with c-signal-dependent gene expression during Myxococcus xanthus development, Proc. Natl. Acad. Sci. U.S.A. 118, e2111706118 (2021).
- [32] P. D. Curtis, J. Atwood III, R. Orlando, and L. J. Shimkets, Proteins associated with the Myxococcus xanthus extracellular matrix, J. Bacteriol. 189, 7634 (2007).
- [33] W. Hu, L. Li, S. Sharma, J. Wang, I. McHardy, R. Lux, Z. Yang, X. He, J. K. Gimzewski, Y. Li *et al.*, DNA builds and strengthens the extracellular matrix in Myxococcus xanthus biofilms by interacting with exopolysaccharides, PLoS One 7, e51905 (2012).
- [34] P. J. Bonner, W. P. Black, Z. Yang, and L. J. Shimkets, FibA and PilA act cooperatively during fruiting body formation of Myxococcus xanthus, Mol. Microbiol. **61**, 1283 (2006).
- [35] R. Lux, Y. Li, A. Lu, and W. Shi, Detailed three-dimensional analysis of structural features of Myxococcus xanthus fruiting bodies using confocal laser scanning microscopy, Biofilms 1, 293 (2004).
- [36] J. W. Arnold and L. J. Shimkets, Inhibition of cell-cell interactions in Myxococcus xanthus by congo red, J. Bacteriol. 170, 5765 (1988).
- [37] B. W. Peterson, H. C. van der Mei, J. Sjollema, H. J. Busscher, and P. K. Sharma, A distinguishable role of eDNA in the viscoelastic relaxation of biofilms, MBio 4, e00497.
- [38] A. E. Pelling, Y. Li, W. Shi, and J. K. Gimzewski, Nanoscale visualization and characterization of Myxococcus xanthus cells with atomic force microscopy, Proc. Natl. Acad. Sci. U.S.A. 102, 6484 (2005).
- [39] P. A. Pinzón-Arango, R. Nagarajan, and T. A. Camesano, Effects of l-alanine and inosine germinants on the elasticity of bacillus anthracis spores, Langmuir **26**, 6535 (2010).
- [40] T.-H. Fang, S.-H. Kang, Z.-H. Hong, and C.-D. Wu, Elasticity and nanomechanical response of Aspergillus niger spores using atomic force microscopy, Micron 43, 407 (2012).
- [41] J. N. Wilking, T. E. Angelini, A. Seminara, M. P. Brenner, and D. A. Weitz, Biofilms as complex fluids, MRS Bull. **36**, 385 (2011).